JOURNAL OF GEOPHYSICAL RESEARCH, VOL. 100, NO. A9, PAGES 17,189–17,203, SEPTEMBER 1, 1995

One- and two-dimensional simulations of whistler mode waves in an anisotropic plasma

P. E. Devine and S. C. Chapman

Space Science Centre, School of Mathematical and Physical Sciences, University of Sussex, Brighton, England

J. W. Eastwood

Atomic Energy Authority, Culham Laboratory, Abingdon, Oxfordshire, England

Abstract. We present results from self-consistent, one- and two-dimensional, electromagnetic simulations of the electron whistler mode instability relevant to the near-Earth nightside plasma sheet region during geomagnetically disturbed times. Specifically, we study the evolution of energetic, anisotropic ($T_\perp > T_{//}$) electron distributions that are injected into the nightside ring current region at geomagnetically disturbed times, the resulting growth of electron whistler mode waves, and subsequent electron pitch angle diffusion via electron whistler wave-particle interactions. Growth of whistler mode waves from an initial pitch angle anisotropy ($T_\perp \approx 4T_{//}$) is studied in the strong pitch angle diffusion regime (defined as having scattering times much shorter than a typical electron bounce time in the near Earth's dipolar field). The quasi-linear and subsequent nonlinear evolution of waves and the corresponding migration of electrons in velocity space is followed over timescales such that ion motion may be neglected. Our simulations contain wave frequencies and growth rates that are a significant fraction of the electron gyrofrequency ($\omega \sim 0.5\omega_{ce}$, $\gamma \sim 0.1\omega_{ce}$ being typical) and the simultaneous evolution of waves propagating both parallel and nonparallel to the ambient magnetic field direction. Effects due to these are not usually accounted for in applications of quasi-linear theory to the problem of electron whistler wave-particle interactions, so that our self-consistent simulations of the electron whistler instability provide an important insight into the applicability of quasi-linear theory to the velocity space diffusion of electrons due to electron whistler wave-particle interactions. We examine the dependence of whistler mode wave growth rates, nonlinear wave mode saturation, and pitch angle diffusion rates on the β value of the hot electron species which contains the resonant population, and we compare the differences between results of one- and two-dimensional simulations. In general, we have found significantly larger average growth rates in a one-dimensional than in a two-dimensional geometry, by up to a factor of ~2-3, with the difference between such growth rates becoming larger as β increases. As a result, we find pitch angle diffusion rates are significantly larger (by up to a factor of ~10) in a one-dimensional geometry, and pitch angle diffusion rates increase as β increases. During the early wave growth period of the instability, pitch angle diffusion rates D_α have been found to scale to magnetic wave energy B_w^2, approximately $D_\alpha \propto B_w^2$. We also show that in the self-consistently evolved system (containing several wave modes), the pitch angle diffusion is still consistent with a usual quasi-linear approach in which resonant particles are taken to diffuse along surfaces of constant wave frame energy.

Introduction

Magnetospheric whistler mode wave-particle interactions (WPIs) have received much attention since *Dungey* [1963] suggested that the pitch angle diffusion driven by lightning-generated whistler waves could occur for radiation belt electrons. *Kennel and Petschek* [1966] proposed that the radiation belt's trapped particle loss cone distributions, which are anisotropic in velocity space, may themselves generate whistler mode waves, which then interact with the particles via WPIs.

Paper number 95JA00842.
0148-0227/95/95JA-00842$05.00

Considerable work has addressed the pitch angle diffusion of electrons due to whistler mode wave-particle interactions. Quasi-linear theory has been applied to predict the growth of whistler waves from and the effect of whistler mode wave-particle interactions on anisotropic magnetospheric electron distributions (having a characteristic temperature perpendicular to the magnetic field ($T_\perp$) exceeding that parallel to the magnetic field ($T_{//}$)) [e.g., *Roux and Solomon*, 1971]. Application of quasi-linear theory to the pitch angle diffusion of electrons has often been restricted by the following assumptions: (1) small wave amplitudes (i.e., in the limit of growth rates $\gamma \to 0$), (2) usually with wave frequencies $\omega \ll \omega_{ce}$ (electron gyrofrequency ω_{ce}), (3) usually neglecting energy diffusion of electrons (pure pitch angle diffusion), and (4) a wave spectrum usually containing waves propagating parallel to the magnetic field only. Such applica-

tion has found success in describing the pitch angle diffusion (and precipitation rates) of electrons inside the plasmasphere, where assumptions (1)-(3) are reasonably well satisfied [e.g., *Lyons et al.*, 1972]. Although most quasi-linear applications have retained restriction (4) above, the importance of including a full (nonmonochromatic) wave spectrum containing both parallel and non-parallel propagating waves has been stressed [*Lyons et al.*, 1972].

Outside the plasmasphere, the validity of these usual assumptions is less clear, particularly during geomagnetically disturbed times. During a substorm, populations of electrons are transported from the magnetotail into the near-Earth ring current region, gaining in energy and anisotropy (a characteristic temperature perpendicular to the magnetic field exceeding that parallel, $T_\perp > T_{//}$) [e.g., *Ashour-Abdalla and Cowley*, 1974]. Whistler mode wave growth should be enhanced at such times, leading to a larger rate of pitch angle scattering into the loss cone and therefore an increased auroral precipitation. *Kremser et al.* [1986] observed an increase in electron precipitation rate corresponding to a period of enhanced electron whistler mode wave intensity during a magnetic substorm, the enhanced precipitation therefore seemingly consistent with pitch angle diffusion due to electron whistler waves (at enhanced levels due to growth from anisotropic electron distributions). Whistler mode wave energy peaks at much higher frequencies (relative to the local electron gyrofrequency) than inside the plasmasphere, frequencies $\omega \sim 0.25$-$0.5\,\omega_{ce}$ being typical outside the plasmapause. The validity of the usual assumptions such as pure pitch angle diffusion and parallel propagating waves needs to be investigated, a quantitative understanding of the degree to which a usual quasi-linear application explains the electron pitch angle diffusion in this regime is of prime importance to the question of the disturbed-time aurora, since the electron whistler instability is believed to be an important mechanism by which energetic electrons are precipitated to form the disturbed-time nightside aurora.

Computer simulation represents a useful tool with which to examine the quasi-linear diffusion and subsequent nonlinear evolution of unstable distributions. Previous whistler instability simulations have been performed in one-dimension (1-D) [e.g., *Ossakow et al.*, 1972; *Cuperman and Salu*, 1973; *Pritchett et al.*, 1991]. Usually, wave propagation in such simulations is restricted to be parallel to the magnetic field, and therefore resonant WPIs to the $n = -1$ principal cyclotron resonance [*Stix*, 1962]. It is possible to study obliquely propagating waves (nonparallel to the magnetic field) in a 1-D simulation [e.g., *Cuperman and Sternlieb*, 1974; *Zhang et al.*, 1993]. This allows the effects of a restricted set of resonances that include $n \neq -1$ to be investigated; for example, *Zhang et al.* [1993] investigated the growth from an anisotropic electron beam of various electrostatic and electromagnetic wave modes at various propagation angles using a series of 1-D simulations. However, wave propagation is still restricted to a single fixed direction (relative to the magnetic field) in such schemes. The periodic two-dimensional (2-D) simulations presented here allow wave propagation angles both parallel and oblique to the ambient magnetic field direction to be included in the same simulation and therefore allow all other possible resonances ($n \neq -1$) in addition to the principal resonance. Previous two-dimensional electromagnetic simulations have not dealt with the electron whistler instability as is the focus in this paper (e.g. *Matsumoto et al.* [1984] investigated the generation of electrostatic waves in the presence of an energetic electron beam and a monochromatic electron whistler wave). We address the quasi-linear and subsequently nonlinear generation of whistler mode waves due to anisotropic energetic electron distributions in an initially unperturbed background magnetic field, the subsequent evolution of waves and the distribution of electrons, and the differences introduced by a 2-D geometry. This simulation study principally concerns the electron whistler instability in two dimensions for the first time. A combined investigation of pitch angle diffusion rates in separate resonant regions of velocity space and velocity space diffusion surfaces is also presented to address the question of the applicability of quasi-linear theory to the velocity space diffusion of electrons due to whistler WPIs. A dependence of electron pitch angle diffusion rates on the wave energy density in the simulation system is obtained, and the pitch angle dependence of the pitch angle diffusion rate in each of three separate resonant regions of velocity space is investigated, both of which allow for a self-consistent investigation of quasi-linear theory predictions with regard to the electron velocity space diffusion.

We first describe the simulation method and our series of simulation studies. Results from these studies are then presented and discussed.

Simulation Details

Simulation Configuration

A two-dimensional, relativistic, electromagnetic, self-consistent particle-in-cell simulation code has been developed using the virtual particle (VP) method of *Eastwood* [1991]. All three vector components of electromagnetic fields **E**, **B**, and velocity **v** are retained as variables of two spatial dimensions and time. Electrons are represented by a set of computational particles, and here ions are represented by a fixed, charge neutralizing background, although this need not be so for other applications. Effectively, our implementation of the VP scheme differs from the more traditional 2-D electromagnetic particle-in-cell codes [*Birdsall and Langdon*, 1985] only in the method of current assignment from particles to the grid, so that an appropriate grid cell size is Δx equal to the Debye length λ_{De}. This avoids possible nonphysical instabilities [*Birdsall and Langdon*, 1985], while still permitting all physical waves with scale lengths of the order or greater than a Debye length (e.g., Langmuir modes, electron whistler waves).

Our choice of doubly periodic boundary conditions effectively quantizes the wave vectors $\mathbf{k} = (k_x, k_y)$ allowed in the system, resulting in a discrete set of "wave modes": $k_x = \pm(2\pi n_x)/L_x$, where $n_x = 0, 1, 2, \ldots, N_x/2$, with N_x the number of grid cells in the x direction (a similar set results for k_y). We choose system lengths (L_x, L_y) to ensure the allowed wave modes adequately cover the region of $\mathbf{k}$ space that the problem of interest demands (see Figure 1, $\mathbf{k} = (k_x, k_y) \equiv (k_{//}, k_\perp$; see Figures 2 and 3 for a typical resolution of the linearly predicted growth region). The evolution of initially anisotropic distributions can be represented, although the periodic boundary conditions used allow no sources or sinks of particles. However, in our simulations the number of

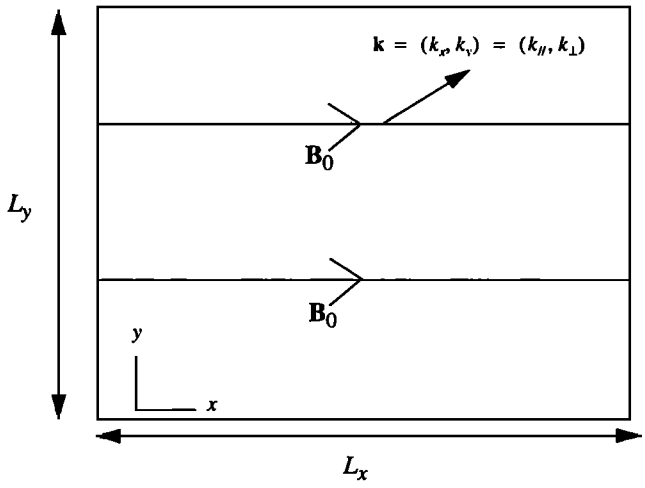

Figure 1. The simulation configuration.

computational particles lying within a typical magnetospheric loss cone (of size $\alpha_0 \approx 5°$) is found to be sufficiently small (~0.1%) such that our results are not found to be affected by including a typical magnetospheric loss cone sink.

The XWHAMP code, a graphically enhanced version of the original waves in homogeneous, anisotropic, multicomponent plasmas (WHAMP) code [*Ronnmark*, 1982], was used to allow comparison of simulation results and linear theory. XWHAMP was used to solve for the linearly predicted complex frequency $\omega = \omega_r + i\gamma$ (ω_r is real frequency, γ is growth rate) over a desired range of $\mathbf{k}$ space, given the following physical parameters: electron cyclotron frequency ω_{ce}, electron plasma frequency ω_{pe}, the parallel electron velocity distribution temperature $k_B T_{//} = 1/2 m v_{th//}^2$, and the perpendicular/parallel temperature ratio $T_\perp/T_{//}$ (a bi-Maxwellian electron velocity distribution function was used, so that $T_\perp/T_{//}$ is the anisotropy of the electron distribution $f(\mathbf{v})$). An example of XWHAMP's results is shown in Figures 2 and 3 respectively, which show the dependence of (ω_r, γ) versus $k_{//}$ (at $k_\perp = 0$) and contour levels of the growth rate $\gamma(\mathbf{k})$ in wave vector $\mathbf{k} = (k_{//}, k_\perp)$ space, for the parameters of our study 1 (to be described next). Both real and imaginary frequencies in Figures 2 and 3 are normalised to the electron gyrofrequency ω_{ce}; this normalization will be used throughout. Also, for the temperature ratio used ($T_\perp/T_{//} \approx 4$), growth rates are a significant fraction of the real wave frequencies (the peak γ_{max} of $\gamma(\mathbf{k})$ is approximately 20% of the real wave frequency at the peak in Figure 2).

Simulation Studies

A set of studies have been performed to investigate the electron whistler mode instability. The simulation configuration is sketched in Figure 1, with an initially uniform magnetic field $\mathbf{B}_0$ in the x direction. In each simulation, the run time was chosen to be $10\tau_{ce}$ electron gyroperiods, that is, run time much less than an ion gyroperiod.

The set of four studies contains a single, hot (tens of keV) resonant electron species with an initially anisotropic ($T_\perp/T_{//} \approx 4$) bi-Maxwellian velocity distribution $f(\mathbf{v})$. The difference between the four studies lies in the choice of electron species temperature and the value of $|\mathbf{B}_0|$; that is, in the β value of the resonant electron species (where $\beta = n_e k_B T/(B_0^2/2\mu_0)$ is the usual ratio of kinetic/magnetic pressure). Parameters are listed in Table 1. Each of the four studies was performed in both 1-D and 2-D. The quantity A represents the electron species anisotropy ($A = T_\perp/T_{//} - 1$), and $\beta_{//} = n_e k_B T_{//}/(B_0^2/2\mu_0)$ is just the parallel β value of the electron species. In all studies, the density of the simulation electron species was taken to represent an electron plasma frequency of $\omega_{pe} = 10^5$ rad s^{-1}.

In all runs, the number of simulation particles was chosen to ensure that the velocity distribution $f(\mathbf{v})$ was represented adequately. A temperature ratio of $T_\perp/T_{//} = 4$ is somewhat large in magnetospheric terms. This was chosen to ensure that whistler mode growth rates exceed nonwhistler noise level growth rates. For the purpose of this study, this noise consists of statistical fluctuations in computational particle populations, electron plasma oscillations, and the bremsstrahlung radiation present in the system (and all of which are enhanced in the simulation, relative to a real system, due to using far fewer computational than there are real particles). Nonwhistler noise was kept to a reasonable level using 144 computational particles per cell on a 128 x 128 cell grid in 2-D runs, and 256 per cell on a 128 x 1 cell grid in 1-D runs. Each of the studies was repeated (in both 1-D and 2-D) using an isotropic electron $f(\mathbf{v})$ of the same overall temperature. These isotropic runs are stable to the whistler instability, and therefore reproduce the above noise fields only and at similar levels that are present in the relevant study. This allows us to make an estimate of noise effects with regard to our results. A lower number of 144 particles/cell in 2-D nevertheless results in a larger total number of particles than in 1-D. The higher number of 256 particles per cell in 1-D gives an improved representation in velocity space over the entire population (i.e., over the whole system) than would be obtained in 1-D with 144 particles per cell, and therefore improves (relative to 1-D 144/cell) the statistics of any quantity calculated over the whole 1-D system (e.g., our pitch angle diffusion calculations). Such calculations can then be more readily compared between 1-D and 2-D. System lengths (L_x,L_y) were chosen to ensure that an acceptable minimum number of allowed (dis-

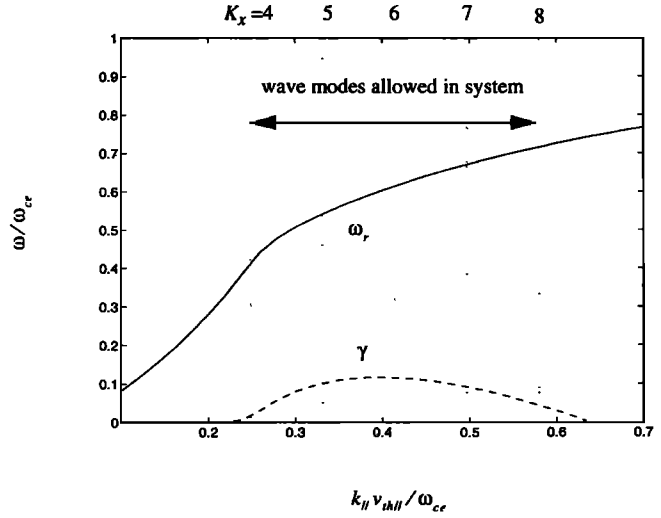

Figure 2. Linear theory parallel dispersion ($k_\perp = 0, K_y = 1$) for our study 1. Dotted lines show the growth modes represented in the simulation (only parallel modes are shown). Calculations were made using the XWHAMP code (see text).

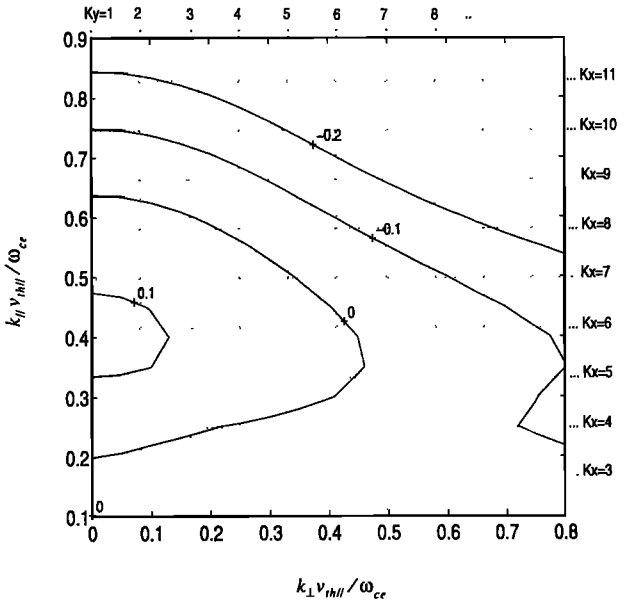

Figure 3. Contour levels of the linearly predicted growth rate $\gamma(\mathbf{k})/\omega_{ce}$ in the wave vector plane **k** for study 1. Dotted lines show wave modes represented in the simulation. Calculations were made using the XWHAMP code (see text).

crete) wave modes fell within the linearly predicted growth region in **k** space (typically >5 modes in 1-D, >10 modes in 2-D); use of the XWHAMP code allowed the resolution of the **k** space growth region ($\gamma > 0$) to be inferred (see Figures 2 and 3).

Results

We will first discuss in detail results from study 1 to compare 1-D and 2-D results at a single $\beta_{//}$.

Evolution of Magnetic Wave Energy in the System

Initially, the magnetic wave energy in the system grows exponentially (see Figure 4b for the magnetic wave energy density in the simulation system), that is, according to linear theory. The growth of wave energy is accompanied by a decrease in both the electron species kinetic energy and the electron species anisotropy (see Figure 4); that is the system moves toward isotropy and hence a decreasing amount of "free" energy available for wave growth. Eventually (by $t \approx 5 - 6\tau_{ce}$ (1-D) and $8\text{-}9\tau_{ce}$ (2-D)), the wave energy saturates at an almost constant level, see Figure 4b. The total energy in the system is conserved to within better than 0.005% over the entire run (as expected for our boundary conditions such that no loss of energy occurs), and by $10\tau_{ce}$ the magnetic wave energy density has reached ~3.1% (1-D) and ~1.9% (2-D) of the initial electron species kinetic energy density (although in higher β studies, the 1-D saturation wave energy is not always larger than it is in 2-D). Note that the average growth rate is larger in a 1-D run than in a 2-D run with the same $\beta_{//}$ value (see Figure 4b). From Figure 4b, taking the spatially averaged magnetic wave energy density in the system to vary as $\mathbf{B}^2_{wave} \propto \exp(2\bar{\gamma}t)$, the average growth rate of the magnetic wave amplitude in 1-D study 1 is estimated to be $\bar{\gamma}_{1D} = (0.076 \pm 0.001)\,\omega_{ce}$, while in the 2-D study 1 it is $\bar{\gamma}_{2D} = (0.054 \pm 0.016)\,\omega_{ce}$. For linear comparison purposes, the XWHAMP-predicted mean of the growth rates of all simulation wave modes lying within the linearly predicted growth region (see Figures 2 and 3) is approximately $0.074\omega_{ce}$ (1-D) and $0.053\omega_{ce}$ (2-D), so that the growth in the magnetic wave energy density at early times is to a good approximation the mean growth rate from linear theory. This means there is negligible wave mode coupling during the early time stages of the instability (in both 1-D and 2-D), and hence the difference in 1-D/2-D growth rates is consistent with linear theory also. In a 1-D geometry, all wave energy is constrained to one of the allowed parallel propagating wave modes, which have relatively higher growth rates (for the same value of $k_{//}$) than the nonparallel wave modes (which suffer from Landau damping [e.g., *Kennel & Petschek,* 1966]) that are present in a 2-D geometry, hence the higher average 1-D growth rates and wave levels. The anisotropy consequently falls faster in the early stages of the 1-D run than in the 2-D run (see Figure 4c). This is due to the higher wave levels in 1-D than in 2-D over that time period.

Growth of Dominant Wave Mode

Looking first at the growth of wave mode energies in the 1-D study 1. Early in the run, the wave spectrum is quite turbulent in that many wave modes grow in energy (see Figure 5). The convenient dimensionless K_x values assigned to the wave modes in Figure 5 are related to the unnormalized parallel wavenumber $k_{//}$ by $K_x = 1 + (L_x\,|k_{//}| / 2\pi)$. As no electron beam is present in the electron velocity distribution $f(\mathbf{v})$, growth rates of waves are expected to be symmetric parallel/antiparallel to the background magnetic field; that is, wave modes having the same $k = |\mathbf{k}|$, but oppositely directed **k**, should grow at the same rate (within noise uncertainties). Each of the mode energies shown in Figure 5 contains both the parallel/antiparallel energy in the two oppositely directed wave modes having the same |k| (each has $k_{\perp} = 0$ (dimensionless $K_y = 1 + (L_y\,|k_{\perp}| / 2\pi) = 1$), since we are considering

Table 1. Physical Parameters for the Studies

Study	Parallel Electron Temperature $k_B T_{//}$, keV	Anisotropy A	$\lvert\mathbf{B}_0\rvert$, nT	$\beta_{//}$	$\frac{\omega_{ce}}{\omega_{pe}}$
1	8.82 keV	2.89	284	0.14	0.5
2	3.56 keV	2.95	100	0.45	0.176
3	6.91 keV	2.91	70	1.79	0.123
4	8.81 keV	2.89	56.9	3.45	0.1

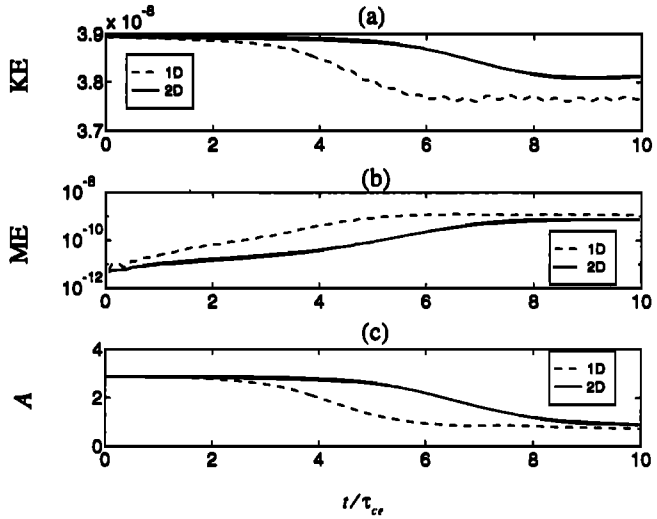

Figure 4. Variation with time of (a) kinetic energy density (KE), (b) average magnetic wave energy density (ME), and (c) electron species anisotropy A during 1-D and 2-D study 1. Note that units of energy densities are J m^{-3}.

a 1-D geometry). The results show different wave modes growing at different rates. Numerically obtained real and imaginary (growth) wave mode frequencies for individual wave modes agree fairly well with linear theory (XWHAMP) predictions during the early stages of the run. For example, the approximate growth rates (normalised to ω_{ce}) of wave modes $K_x = 5$, 6 are 0.1 ±10% and 0.11 ±20%, respectively, while the linearly predicted growth rates for these modes are 0.11 and 0.12, respectively.

As wave energy increases and anisotropy decreases, the general trend is for higher |k| modes to saturate in energy and for magnetic energy to shift toward lower |k| modes. From a linear viewpoint (therefore not entirely correct when wave amplitudes have grown significantly), there is a maximum wave mode k_{max} allowed to grow, depending on the current anisotropy, with k_{max} given by *Ossakow et al.* [1972]

$$k_{max} = \frac{\omega_{pe}}{c}\left[(T_\perp/T_{//}) - 1\right]^{1/2} \quad (1)$$

Hence, as k_{max} decreases with decreasing anisotropy ($A = T_\perp/T_{//} - 1$), then as the simulation progresses (A decreases in time) the range of available resonant **k** modes decreases. As k_{max} falls below the initially available higher |k| modes, there is a shift of magnetic whistler mode wave energy towards lower |k| modes. This can be seen from Figure 5, with magnetic energy shifting in time from mode $K_x = 7 \rightarrow 6 \rightarrow 5 \rightarrow 4$. Clearly, when the anisotropy decreases markedly from its initial level, the quasi-linear wave spectrum will not agree exactly with the linearly predicted spectrum, with the maximum of the spectrum being displaced toward a lower frequency than predicted by linear theory. Also seen from Figure 5, eventually (by ~ $8\tau_{ce}$) in 1-D, all modes but one seem to have saturated, and we are left with a single, dominant wave mode ($K_x = 4$) in the system that propagates parallel to the background magnetic field. Note that this dominant wave mode is not the lowest wave mode resolved by the simulation; that is, we are not observing a system-related shift toward ever lower |k| modes until we reach the lowest possible simulation mode. Such a final spectrum, dominated by a single wave mode, could favor saturation of magnetic wave energy by nonlinear magnetic trapping effects, as suggested by *Ossakow et al.* [1972].

Figure 6 shows the magnetic wave profile $B_y(x,t)$ during the early time stages of 1-D study 1. Electron whistler waves propagating parallel to the background magnetic field ($\mathbf{B}_0$ along $\hat{\mathbf{x}}$) are transverse electromagnetic waves right circularly polarized about $\mathbf{B}_0$, so that $B_y(x,t)$ is one of the pair of

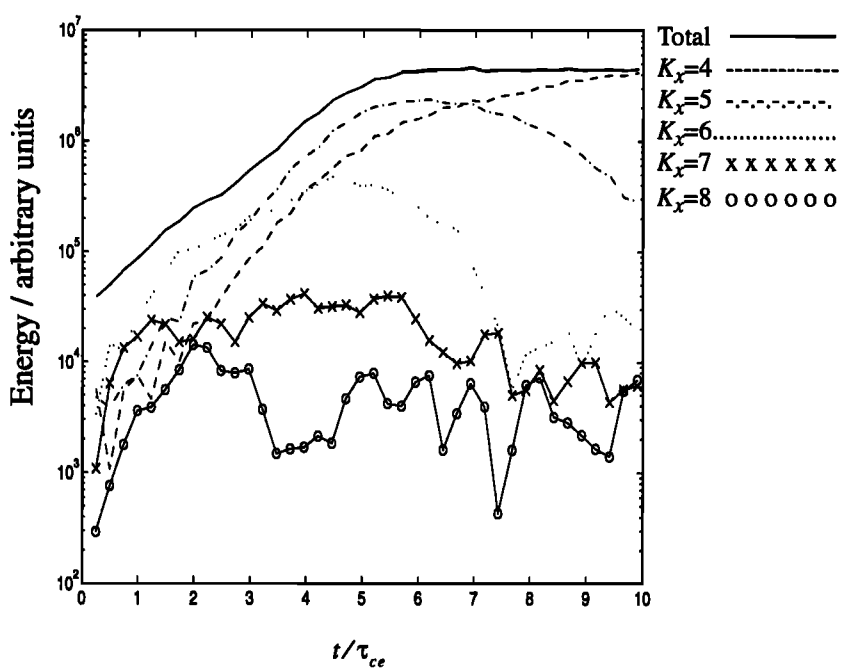

Figure 5. Magnetic energy in resonant wave modes K_x= 4-8 during the 1-D study 1. Other modes in the system contain nonwhistler noise only and do not grow noticeably in time.

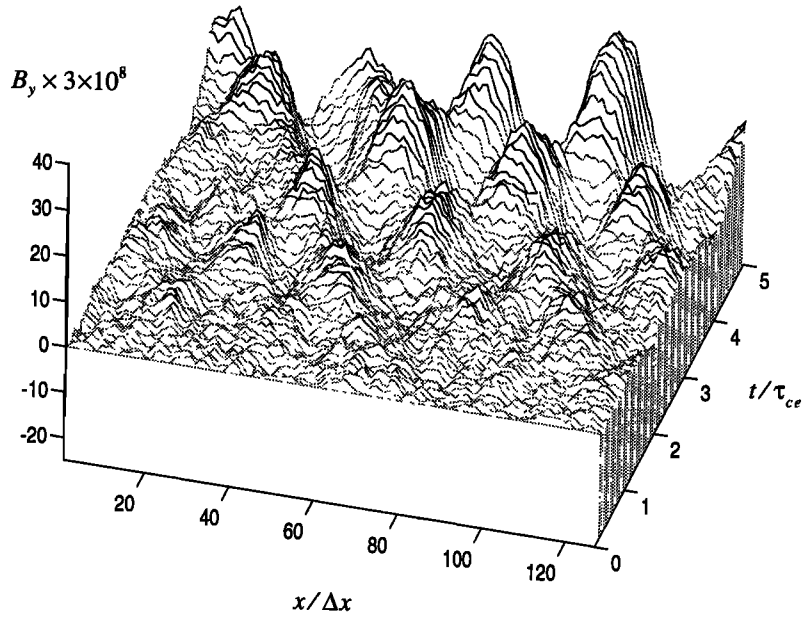

Figure 6. Magnetic wave profile $B_y(x,t)$ during the early time stages of 1-D study 1. Distance x is measured in units of grid cells (Δx); the magnetic wave field amplitude is multiplied by 3×10^8.

circularly polarized components of the magnetic whistler wave field. Hence both the growth of magnetic wave amplitude and the shift in time of wave energy toward longer wavelengths are seen in $B_y(x,t)$ of Figure 6. The resultant wave field $B_y(x,t)$ in the simulation is essentially (excluding noise contributions) the sum $\sum B_{k0} e^{i(\mathbf{k}\cdot\mathbf{r}-\omega t+\phi_k)}$ of all the discrete linearly predicted growth whistler wave mode waves (each of amplitude B_{k0}, wave vector $\mathbf{k}$, frequency $\omega_k = \omega_{rk} + i\gamma_k$, initial phase ϕ_k) propagating both parallel and antiparallel to $\mathbf{B}_0$ ($K_x = 4$ to 8 in Figure 5). From such a set of oppositely propagating waves, together with the periodic boundary conditions employed in the simulations, one may expect a form of standing wave to eventually develop in $B_y(x,t)$, provided a fixed phase relationship between the individual wave modes exists (see *Zhang et al.* [1993] for the case of beating between longitudinal electron plasma waves). However, individual wave modes are expected to be randomly phased, with there being no obvious phase relationship between the different mode ϕ_ks. Hence early in the simulation (approximately $t < 3 - 4\tau_{ce}$), when the wave spectrum contains several wave modes of comparable energy (see Figure 5), the resultant wave field $B_y(x,t)$ in Figure 6 does not appear to be representative of a stationary wave. Later in the run, as the wave spectrum becomes dominated by fewer modes, the resultant wave field approaches the sum of pairs of oppositely propagating waves having roughly equal amplitude (within noise uncertainties) and having a clearer phase relationship.

In 2-D runs the wave spectrum is found to be far more turbulent, since a far greater number of growth wave modes are present. There is no longer the restriction that $k_\perp = 0$ ($K_y = 1$). Instead, a full set of values for the dimensionless perpendicular wavenumber K_y now results as did for K_x. Early in the run, it is found that the region of k-space that grows appreciably agrees well with that predicted by linear theory, with individual wave mode growth rates agreeing fairly well with linear predictions (as in 1-D). Significant energy resides in growing nonparallel ($k_\perp \neq 0$) wave modes (early in the run, up to 90% as much energy resides collectively in nonparallel growth wave modes as in parallel growth wave modes collectively), though of two wave modes having the same $k_{//}$ (K_x) but different $k_\perp$ (K_y), the one with lower $k_\perp$ (i.e., the more parallel (less oblique)) tends to grow faster. This can be seen from Figure 7, which shows the growth in magnetic wave energy for linearly predicted growth wave modes (K_x,K_y), each of the same dimensionless parallel wavenumber $K_x = 5$, and different perpendicular wavenumbers $K_y = 1$-6. A similar trend of magnetic wave energy shifting toward

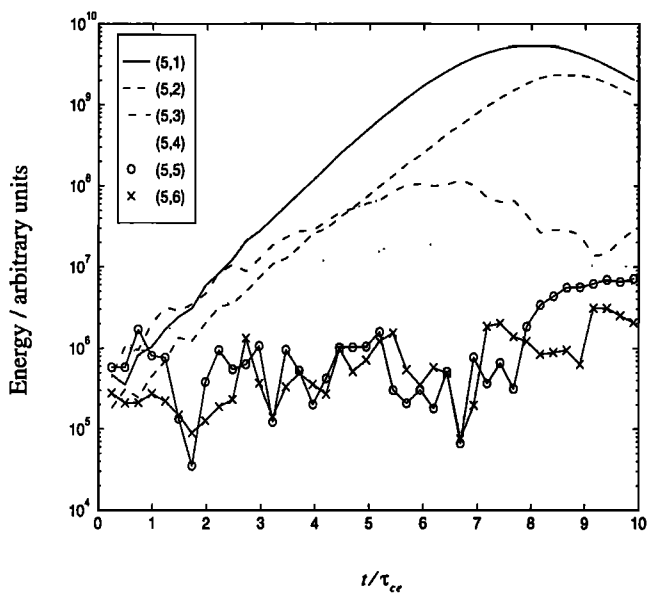

Figure 7. Magnetic energy in resonant growth modes (K_x,K_y) having the same dimensionless parallel wavenumber $K_x = 5$ and different perpendicular wavenumbers K_y, during the 2-D study 1.

lower |k| modes as time progresses is seen in 2-D as was seen in 1-D, with the order of such shifting now being from dominant wave modes having $K_x = 6 \rightarrow 5 \rightarrow 4$. This is best seen from Figure 8, which shows the growth in collective magnetic wave energy at each K_x, summed over all K_y ($k_\perp$); that is, we are plotting the sum $\sum B^2_{K_x K_y}$ over K_y for each K_x. During the $10\tau_{ce}$ run time in 2-D, we do not observe a final spectrum dominated by a single, parallel propagating wave mode in the system (as was seen in 1-D). The energy spectrum late in the run (after ~ $9\tau_{ce}$) is dominated collectively by those wave modes having $K_x = 4$ (see Figure 8). However, this energy is shared roughly equally between the two wave modes $(K_x,K_y) = (4,1)$ and (4,2) (see Figure 9 between 9 and $10\tau_{ce}$). Results obtained by extending the 2-D run time to $20\tau_{ce}$ (see Figure 9 after $10\tau_{ce}$) show that eventually (by ~ $16\tau_{ce}$) the 2-D wave spectrum becomes dominated by a single, large amplitude, parallel propagating wave mode having $(K_x,K_y) = (4,1)$; that is, the same eventual dominant mode of the 1-D study dominates the 2-D study but at a later time (at approximately $8\tau_{ce}$ in 1-D, $16\tau_{ce}$ in 2-D). In both geometries, however, this occurs at a time outside the period for which we expect quasi-linear diffusion to occur, as will be discussed next.

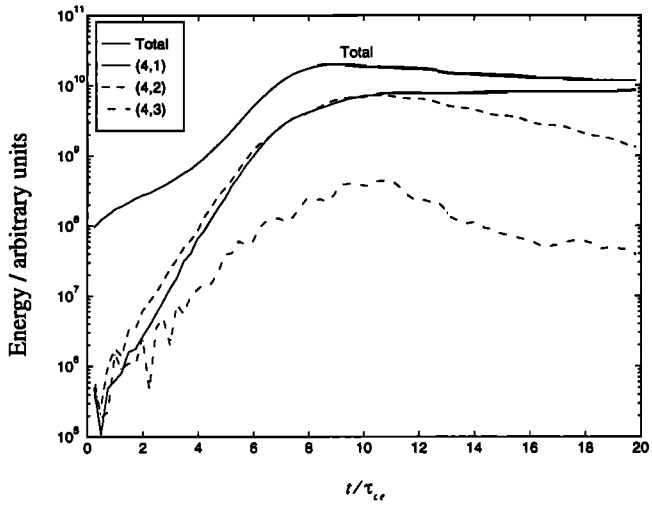

Figure 9. Magnetic energy in resonant growth modes (K_x,K_y) having the same dimensionless parallel wavenumber $K_x = 4$ and different perpendicular wavenumbers K_y, during the 2-D study 1.

Pitch Angle Diffusion: Study 1

In order to investigate the pitch angle diffusion of electrons due to the whistler mode waves present in the system, we have calculated "snapshots" of the local pitch angle diffusion rate in three separate regions of velocity space, at various times during the simulations. These regions were chosen to be velocity space "strips" of width $\pm 10^6$ m s^{-1}, centred at $v_{//} = -7.84 \times 10^7$ m s^{-1}, -5.15×10^7 m s^{-1}, and -3.69×10^7 m s^{-1}. Each of these strips lies within the linearly predicted region of velocity space in which we expect there to be $n = -1$ electron whistler mode resonances with wave modes for which $K_x = 5$, 6, and 7 (these modes are included in Figure 5). In 1-D, since waves propagate parallel to the magnetic field only, these resonances are limited to the three wave modes K_x=5, 6, and 7, all with $K_y = 1$ (or $k_\perp = 0$). In 2-D, $n = -1$ resonances with wave modes of the same $k_{//}$ (K_x) but different $k_\perp$ (K_y) are predicted (by linear theory) to have virtually identical $n = -1$ resonant particle parallel velocities $v_{//res} = (\omega_r - \omega_{ce})/k_{//}$, since the real frequency ω_r shows very little variation (constant within ~2%) with $k_\perp$ at a fixed $k_{//}$ (for the parameters relevant to our studies). Hence in our 2-D studies, our three strips are expected to contain contributions to the local pitch angle diffusion of particles from resonances with a whole set of parallel and nonparallel modes which have dimensionless parallel wavenumbers $K_x = 5$, 6, and 7, respectively. Only regions of velocity space in which are expected electron whistler wave $n = -1$ resonances were selected because only such resonances occur in a 1-D geometry for which whistler waves propagate parallel/antiparallel to the background magnetic field [e.g., *Stix*, 1962], and our aim is to make 1-D/2-D comparisons of pitch angle diffusion rates. The strip width of $\pm 10^6$ m s^{-1} was chosen as narrow enough to allow us to distinguish separate resonances with wave modes having different K_x, while containing a sufficient number of particles to produce meaningful statistics in our calculations (typically several hundred particles lay within a 1-D strip and more than this in 2-D). Henceforth, we shall refer to these three strips as mode 5, mode 6, and mode 7, respectively. To calculate a snapshot of the local pitch angle diffusion rate for a particular mode (henceforth $k_x = K_x = 5$, 6, or 7), over a time interval $(t, t+\tau)$, we first select all particles lying within the mode at time t. At time $(t+\tau)$, we calculate the change in pitch angle ($\Delta\alpha$ in rad) over the period τ for each particle that was in the mode at t. A normalized local pitch angle (p.a.d.) rate $\hat{D}_{\alpha k_x}$ for a mode k_x is then calculated as:

$$\hat{D}_{\alpha k_x} = \frac{\langle (\Delta\alpha)^2 \rangle}{\tau} \left(\frac{1}{f_{ce}}\right), \qquad (2)$$

where the averaging $\langle \ldots \rangle$ is performed over all the particles in the velocity space strip corresponding to the mode of interest, and $\hat{D}_{\alpha k_x}$ (in rad^2), is normalized to the electron gyrofrequency f_{ce}. Our choice of $\tau = 20\Delta t$ simulation time steps

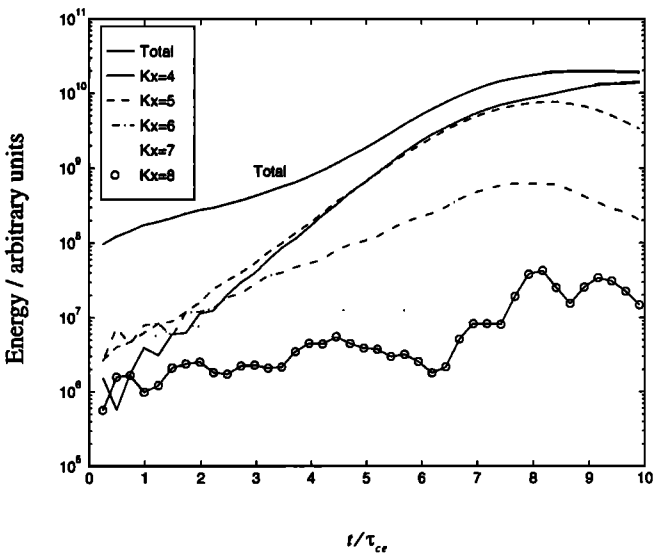

Figure 8. Collective magnetic energy at each K_x, summed over all K_y, for linearly predicted resonant growth modes during the 2-D study 1.

(Δt) represents a small fraction of an electron gyroperiod (typically $\tau < \tau_{ce}/8$), and we calculate $\hat{D}_{\alpha k_x}$ for each of the three modes, roughly 3 times per gyroperiod. Thus a series of snapshots of $\hat{D}_{\alpha k_x}$ is obtained by choosing τ to be much shorter than the time interval over which wave energy is seen to grow (i.e., much shorter than an electron gyroperiod- see Figures 4 and 5 for wave growth). Note that use of a standard quasi-linear approach [*Kennel and Engelmann*, 1966] leads to a diffusion rate that applies to time periods of the order of an electron gyroperiod or more (over which the wave energy is assumed not to grow significantly), since the equation describing the time evolution of $f(\mathbf{v})$ is Larmor-phase-averaged. In our studies, wave energy does not grow significantly over the period τ for which our snapshots of the p.a.d. are calculated. Hence, although our p.a.d. rates are calculated over much shorter time scales than would be done using a quasi-linear approach, we shall see that certain features of the p.a.d. are well-described using such an approach.

Calculated p.a.d. rates $\hat{D}_{\alpha k_x}$ at various times during the early growth period of wave energy in both the 1-D and 2-D runs of study 1 are shown in Figure 10. Figure 11 shows velocity space trajectories, in the simulation rest frame, of 30 of the particles lying within mode 7 at $t = 0$, during the 1-D study 1. From Figure 11 we see that after $t \approx 4.5\tau_{ce}$ individual particle trajectories in velocity space indicate a more pronounced nonlinear behaviour. We identify the end of the period of quasi-linear diffusion by inspection of individual particle phase space trajectories, shown as a vertical dashed line in Figure 11, and only present p.a.d. rates up to this time in Figure 10. In our chosen quasi-linear regime ($t < 4.5\tau_{ce}$), particle trajectories are characterized by slow variations in velocity and energy, though some particles move in v space on a much faster timescale than the "bulk" of particles over the same time period, thereby suggesting that resonance is phase dependent as well as $v_{//}$ dependent. Mean velocity changes are small, hence individual energy exchanges (between wave and particle) are small (based on the average kinetic energy per particle of the entire electron species, a typical electron experiences a net loss in its kinetic energy of ~1% for the chosen time period, which accounts for the growth of wave energy over the same period). As noted earlier, the wave spectrum is turbulent during this time period, and wave-particle interactions with such a spectrum of randomly phased turbulence can be characterized as a stochastic process described by a diffusion equation (see, for example, [*Kennel & Petschek*, 1966] for a treatment of pitch angle diffusion). In our simulations, the turbulent spectrum is effectively represented by a collection of discrete wave modes. However, our resolution of the turbulent spectrum (~5 modes in 1-D, >10 in 2-D) is sufficiently large that the quasi-stochastic process occurs in our chosen quasi-linear regime.

After $t \approx 4.5\tau_{ce}$, the particle dynamics become strongly nonlinear, with much larger changes in particle velocity and energy occurring, and our estimate of p.a.d. in localized regions of phase space is no longer applicable. In this nonlinear regime, the 1-D wave spectrum is essentially dominated by one/two large amplitude wave modes (see Figure 5), and the stochastic description no longer applies. Instead, some particles near resonance may become "trapped" for some time around resonance, seen as oscillations in parallel velocity $v_{//}$ at a "trapping" frequency and centered about the resonant parallel velocity [e.g., *Sudan and Ott*, 1971]. Oscillations in $v_{//}$ are evident in some of the particle trajectories of Figure 11a, and may indicate that trapping effects become important later in the run. At a given time, some of these particles appear to be trapped, while others do not. Although this chosen group of particles are all initialized with the same parallel velocity $v_{//}$, they have different per-

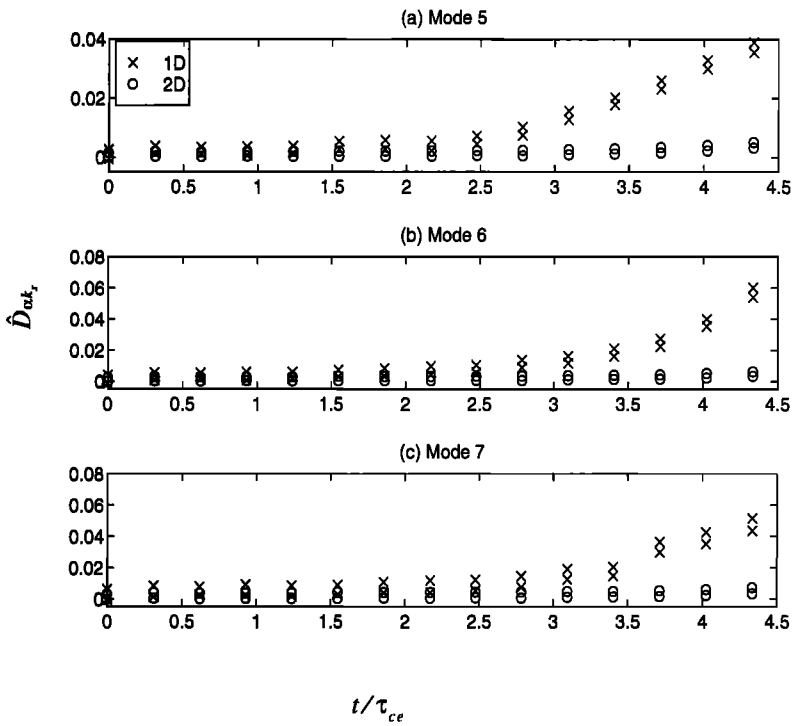

Figure 10. Calculated pitch angle diffusion rates for (a) mode 5, (b) mode 6, and (c) mode 7 regions of velocity space in 1-D (crosses) and 2-D (open circles) study 1.

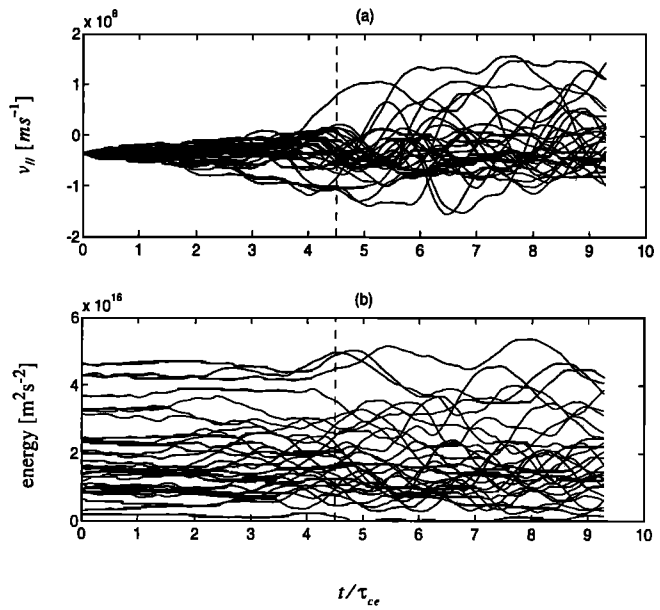

Figure 11. Individual **v** space trajectories of 30 particles in the simulation rest frame, each of which lay within mode 7 at the start of the simulation, in the 1-D study 1, (a) velocity $v_{//}$ and (b) lab frame energy $(v_{//}^2 + v_{\perp}^2)$ versus time.

pendicular velocities and positions. Hence the particles whose trajectories are shown in Figure 11 all start out with different initial velocities and positions and therefore different Larmor phases with respect to the wave fields. As a result, their subsequent phase space motion is markedly different.

Pairs of values of $\hat{D}_{\alpha k_x}$ are presented in Figure 10 to show estimates of the possible uncertainty in the calculated $\hat{D}_{\alpha k_x}$ due to noise wave fields, noise as discussed previously meaning any nonwhistler wave mode not expected to grow from a linear viewpoint. Estimating such uncertainties allows us to identify the pitch angle scattering due solely to whistler mode waves. To estimate uncertainties in $\hat{D}_{\alpha k_x}$ due to noise in a particular study, we repeated the simulations with an initially isotropic electron $f(\mathbf{v})$ to generate similar noise level growth rates. The normalized p.a.d. rates due to nonwhistler noise alone were estimated from each isotropic run, and uncertainties in $\hat{D}_{\alpha k_x}$ are represented by the range of values spanned by the centers of the pairs of symbols in Figure 10. Inspection of p.a.d. rates in Figure 10 then reveals the following:

1. The pitch angle diffusion rate $\hat{D}_{\alpha k_x}$ grows in time as the magnetic wave energy in the system grows. To a reasonable approximation, we have found $\hat{D}_{\alpha k_x} \propto B_w^2$, where B_w^2 is the magnetic wave energy density in the system. For example, over the time period $t \approx (2.5 - 4)\,\tau_{ce}$, the p.a.d. rate $\hat{D}_{\alpha k_x}$ increases by a factor of ~1.7-2.7, while B_w^2 grows by a factor of ~2.2. Such a result is predicted from a quasi-linear approach (see, for example, *Kennel and Petschek* [1966], equation (3.10)).

2. The pitch angle diffusion rate due to whistler mode waves is larger in 1-D than in 2-D for $t > 2\tau_{ce}$. By $4\tau_{ce}$ the p.a.d. rate in 1-D is roughly 10 times that in the 2-D study (the wave energy density in the 1-D study is approximately 10.6 times that in the 2-D study at this time, see Figure 4b). We have already seen how the magnetic wave energy grows more rapidly in 1-D, hence this result is not so surprising, as the p.a.d. rate scales to the magnetic wave energy. Before $2\tau_{ce}$, nonwhistler noise in $\hat{D}_{\alpha k_x}$ renders the 1-D and 2-D results indistinguishable.

3. Nonwhistler noise effects prevent us from distinguishing the whistler-produced p.a.d. rates in the three different regions of **v** space. Since we have used more than 100 particles/cell in our simulations (almost 2.5 million total number in 2-D), and with the net nonwhistler noise in the code having been observed to scale to $1/N_{\text{pcell}}$ (N_{pcell} = number of particles/cell), a further reduction in this effect can not be realistically achieved with this or similar particle-in-cell computational techniques without the use of a noise reduction technique(s) that significantly lowers the noise level.

In addition to the p.a.d. calculations described above, we have made an additional set of study 1 calculations in which the p.a.d. rate $\hat{D}_{\alpha k_x}$ is investigated as a function of pitch angle $\alpha = atan\,(v_{\perp}/|v_{//}|)$, that is, $\hat{D}_{\alpha k_x}(\alpha)$ is investigated, within each of the three modes $k_x = 5$, 6, and 7. Because of the pitch angle anisotropy of the simulation electron species, the number of simulation particles at small pitch angles is relatively small. This would lead to large statistical uncertainties in $\hat{D}_{\alpha k_x}(\alpha)$ at small α if we attempted to calculate $\hat{D}_{\alpha k_x}(\alpha)$ using the simulation electron species. Hence we have chosen to calculate $\hat{D}_{\alpha k_x}(\alpha)$ by using a set of 10,000 "tracer" particles per mode, each of which is moved according to the wave fields present in the system but does not actually contribute to the wave fields. Such particles allow us to uniformly populate velocity space regions of interest in large enough numbers that statistical problems can be overcome. To calculate $\hat{D}_{\alpha k_x}(\alpha)$ for a particular mode k_x over the time interval $(t, t+\tau)$, we first load the 10,000 tracer particles uniformly in perpendicular velocity $v_{\perp}$ at the center of the mode ($v_{//}$ = const.), at the time t. These particles are tagged, according to their pitch angle, into one of a number of 5° bins covering the range $\alpha = 0$ to 90°. At time $(t+\tau)$, the normalized p.a.d. rate is calculated in each bin, as in (2) but now with the averaging being performed over all particles lying within the bin at time t. To complete this set of calculations, the nonwhistler noise-produced p.a.d. in each bin was estimated in the relevant isotropic noise level run, thereby allowing an estimate to be made of the p.a.d. as a function of pitch angle in each mode k_x due solely to electron whistler WPIs.

Before looking at the results of such calculations, we shall consider the p.a.d. process within one of our modes in some detail and make some predictions regarding the expected variation in $\hat{D}_{\alpha k_x}(\alpha)$. We shall first concentrate on the p.a.d. in a 1-D geometry. Mode calculations show the average change in a particle's wave frame energy to be conserved within ~4% during the period τ over which our p.a.d. rates are calculated for the 1-D study 1 (and conserved within less than this in 2-D). Hence we consider particles to move along a diffusion surface of constant energy in the relevant wave frame during the period τ over which p.a.d. rates are calculated. Denoting the parallel component of the wave phase-velocity as $v_{//w}$, then such a surface is described by $(v_{//} - v_{//w})^2 + v_{\perp}^2 = \text{const}$, and is a usual feature of a quasi-linear treatment [e.g., *Lyons*, 1974]. Figure 12 shows the geometry of a mode in phase space. With reference to Figure 12, we may write the displacement Δ of a resonant particle along its diffusion surface as

$$\Delta = v_L \Delta\alpha_L \hat{\mathbf{e}}_{\alpha} + \Delta v_L \hat{\mathbf{e}}_v,$$

where (v_L, α_L) are the particle's lab frame (rest frame)

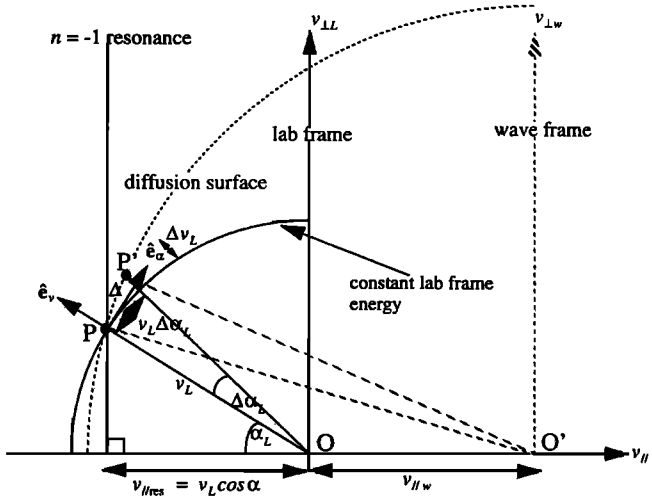

Figure 12. A simplistic sketch showing the diffusion of a resonant particle along its diffusion surface. The displacement of the particle along this surface is represented by Δ. Dashed lines and subscripts w indicate the wave frame, subscripts L indicate the lab frame (simulation rest frame).

velocity and pitch angle, $(\Delta v_L, \Delta\alpha_L)$ the changes in these quantities, and $(\hat{e}_v, \hat{e}_\alpha)$ are unit vectors in the direction of increasing velocity and pitch angle, respectively. Note a rather exaggerated displacement Δ has been used in Figure 12 in order that the geometrical effects of the p.a.d. process may be seen clearly. Since all particles within the same mode have the same parallel velocity $v_{//} = v_{//res}$, then we may substitute for a particle's velocity v_L within a mode

$$v_L = \frac{v_{//res}}{cos\alpha}$$

This is a geometrical effect due to the strip nature of a resonant mode in **v** space. We wish to solve for the variation in $\Delta\alpha_L$ with α_L within a given mode. Approximately (see Figure 12)

$$(v\Delta\alpha)^2 = \Delta^2 - (\Delta v)^2,$$

where we are henceforth dropping subscripts L for convenience.

Now assuming a fixed displacement Δ for all particle pitch angles within the mode (reasonable, since in a 1-D geometry all particles within the same mode are resonant with the same wave mode) and substituting for $v = v_L = v_{//res}/cos\alpha$, then we have

$$(\Delta\alpha)^2 = [(\Delta)^2 - (\Delta v)^2] \frac{(cos\alpha)^2}{v_{//res}^2}$$

From this expression, the variation in the normalized p.a.d. rate $\hat{D}_{\alpha k_x}(\alpha)$ (see (2)) with pitch angle, within a given mode k_x, can be predicted

$$\hat{D}_{\alpha k_x} = \frac{(\Delta\alpha)^2}{\tau}\left(\frac{1}{f_{ce}}\right) = [(\Delta)^2 - (\Delta v)^2] \frac{(cos\alpha)^2}{v_{k_x//R}^2 \tau f_{ce}} \quad (3)$$

where the velocity $v_{k_x//R} = v_{//res}$ is taken to be the resonant parallel velocity for the mode (k_x) of interest.

Often, the limit $|v_{//res}| \gg |v_{//w}|$ (note a $n = -1$ resonant particle and the corresponding wave have oppositely directed velocity components along the background magnetic field) is taken in a quasi-linear theoretical approach [e.g., *Kennel and Petschek*, 1966]. In this case, we can imagine the origin of the wave frame O' in Figure 12 being taken close toward the origin O of the lab frame. As a result, the diffusion surfaces approach surfaces of constant lab frame energy, the change in lab frame velocity Δv is very small compared to the displacement Δ along the diffusion surface ($(\Delta v)^2 \ll \Delta^2$ in (3)), and pure pitch angle diffusion occurs. In our simulations, a ratio $|v_{//res}/v_{//w}| \sim 1$ is typical (as depicted in Figure 12). However, even with such a ratio, at low pitch angles the diffusion surfaces will approach surfaces of constant lab frame energy, and pure pitch angle diffusion should be a good approximation, that is, at low particle pitch angles within one of our modes (k_x) we expect

$$\hat{D}_{\alpha k_x} = \left(\frac{\Delta}{v_{k_x//R}}\right)^2 (cos\alpha)^2 \left(\frac{1}{\tau f_{ce}}\right) \quad (4)$$

Comparing (3) and (4), we see that Δv represents a correction to the pure pitch angle diffusion approach, so as to take into account the geometrical effect of a displacement along a diffusion surface of constant energy in the resonant wave frame, that does not in general coincide with a surface of constant lab frame energy. Such a geometrical effect is allowed for in the quasi-linear calculations of *Lyons* [1974], since no assumption is made about the ratio $|v_{//res}/v_{//w}|$. Hence we use the pitch angle diffusion coefficient of *Lyons* [1974] to predict the variation in the normalized p.a.d. rate $\hat{D}_{\alpha k_x}(\alpha)$ with pitch angle α, within a given mode k_x, and over the full pitch angle range. This was done by using *Lyons'* equation (6) for the p.a.d. coefficient $D_{\alpha\alpha}^{nk_\perp}$ applicable to a resonance of a given order n ($n = -1$ for our interests), with a resonant wave mode of perpendicular wavenumber $k_\perp$ (and at a given $k_{//}$). Since *Lyons'* definition of the p.a.d. coefficient is $D_{\alpha\alpha}^{nk_\perp} \sim (v\Delta\alpha)^2/(2\Delta t)$ (Δt being an appropriate scattering time), use of the relation $v = v_{k_x//R}/cos\alpha$ within a given mode allowed the variation in our normalized p.a.d. rate $\hat{D}_{\alpha k_x}(\alpha) = \langle(\Delta\alpha)^2\rangle/\Delta t$ to be predicted for each of our modes. The result is

$$\hat{D}_{\alpha k_x} \propto (\omega_{ce}/\omega_{k_x} - (sin\alpha)^2)^2, \quad (5)$$

where ω_{k_x} is the real frequency of the relevant mode k_x of interest, and the constant of proportionality in (5) contains the energy of the resonant wave mode.

In order to see whether the p.a.d. occurring within our simulation can be described using the simple geometrical approach described above, we have calculated the predicted variation in $\hat{D}_{\alpha k_x}(\alpha)$ within each of our three chosen resonant modes, using both the pure pitch angle diffusion approximation (see (4)) and the full-diffusion *Lyons'* based equation (5). To be able to predict $\hat{D}_{\alpha k_x}(\alpha)$ using (5), the real frequency ω_{k_x} of each mode k_x was taken from the linearly predicted dispersion $(\omega, k_{//})$ for each mode (see Figure 2).

Tracer-obtained results are presented in Figure 13 for the p.a.d. $\hat{D}_{\alpha k_x}(\alpha)$ at $t \approx 2.5\tau_{ce}$. Nonwhistler noise error bars have been used rather than pairs of values and represent the

estimated uncertainty in $\hat{D}_{\alpha k_x}(\alpha)$ due to nonwhistler noise, calculated from a set of tracers within the relevant isotropic noise level run. Note again that we are considering the 1-D study 1. Clearly, within a particular mode, the p.a.d. rate $\hat{D}_{\alpha k_x}$ decreases with increasing α, as we would expect based on either (4) or (5). For each mode shown in Figure 13, two curves have been drawn to represent the variation in $\hat{D}_{\alpha k_x}(\alpha)$ as predicted by the pure pitch angle diffusion approximation (4) and the full-diffusion *Lyons'* based equation (5). The unknown "amplitude" of variations of each of the curves ($(\Delta/v_{k_{x/\!/R}})^2/(\tau f_{ce})$ in (4)) was chosen by trial and error to give a reasonable-looking fit to the simulation results (for a particular mode, the amplitude of the two curves was taken to be the same). From Figure 13, it can be seen that, in general (though most noticeably in mode 5, which has the largest ratio $|v_{/\!/res}/v_{/\!/w}| \approx 0.88$ of the three modes), at pitch angles less than about $\alpha < 50° - 60°$, there are not significant differences (within noise uncertainties) in the agreement with the simulation-obtained results of the two separate prediction curves based on (4) and (5). Recalling that derivation of (4) used a pure pitch angle diffusion approximation, it can be seen (Figure 13) that for pitch angles below $\alpha < 50° - 60°$, the pitch angle diffusion within our three resonant modes is well-described by a pure pitch angle diffusion approach. The pure pitch angle diffusion approximation becomes less accurate, within noise uncertainties, in all modes above $\alpha > 65°$. The agreement with *Lyons'* predictions (our (5)) is such that the predicted curves pass through all simulation-obtained results (within noise uncertainties) in mode 5 and all but two/one in modes 6 and 7.

In attempting to apply these descriptions to tracer-obtained results for the p.a.d. $\hat{D}_{\alpha k_x}(\alpha)$ in the 2-D study 1, we found that an unacceptably large level of noise uncertainty (~±25%) in $\hat{D}_{\alpha k_x}(\alpha)$ prevented us from distinguishing the quality of the fit of each of the two prediction curves to simulation-obtained results. A higher relative noise uncertainty in $\hat{D}_{\alpha k_x}(\alpha)$ is present in 2-D than in 1-D during our chosen quasi-linear period because there is a larger level of nonwhistler noise in a 2-D simulation (e.g., 2-D allows electron plasma oscillations in more than just one fixed direction). Also, as has already been seen, the 2-D whistler wave energy grows more slowly than in 1-D. Hence a longer period of time is necessary for 2-D whistler wave levels to grow sufficiently over nonwhistler noise levels for this comparison, by which time we are outside the chosen quasi-linear period of $4.5\tau_{ce}$ (the chosen quasi-linear period based on 1-D particle dynamics). Nevertheless, 2-D p.a.d. results show the same general trend of a decreasing p.a.d. rate $\hat{D}_{\alpha k_x}$ as the pitch angle α increases within a mode, consistent with $\hat{D}_{\alpha k_x}(\alpha) \sim (cos\alpha)^2$ (see (4)).

Effect of Increasing $\beta_{/\!/}$: Studies 2 - 4

As we increase the $\beta_{/\!/}$ value of the electron species, we observe larger average magnetic wave energy growth rates (see Figures 14a and 15a), as predicted by linear theory. The average growth rates presented in Figure 15a were calculated from the growth of average magnetic wave energy (Figure 14a) in the same manner as described earlier for study 1 results and represent an average growth rate of magnetic

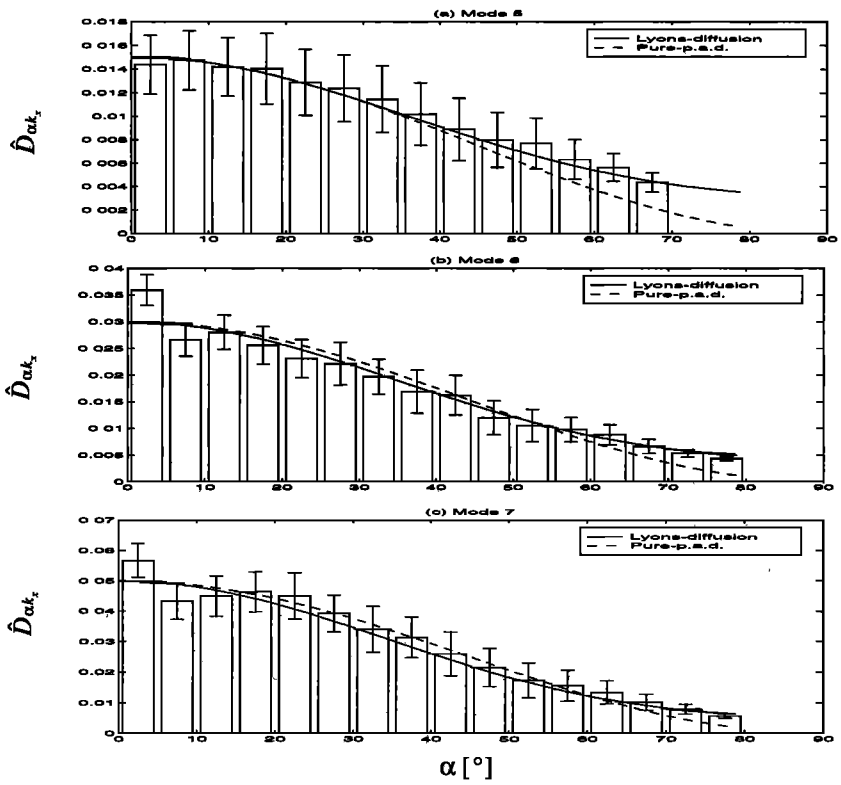

Figure 13. Variation in the tracer-obtained p.a.d. rates $\hat{D}_{\alpha k_x}(\alpha)$ with pitch angle α in (a) mode 5, (b) mode 6, and (c) mode 7 regions of velocity space at $t \approx 2.5\tau_{ce}$ during the 1-D study 1. For each mode, the dashed and solid curves represent the predicted variation in $\hat{D}_{\alpha k_x}(\alpha)$ based on our (4) and (5), respectively.

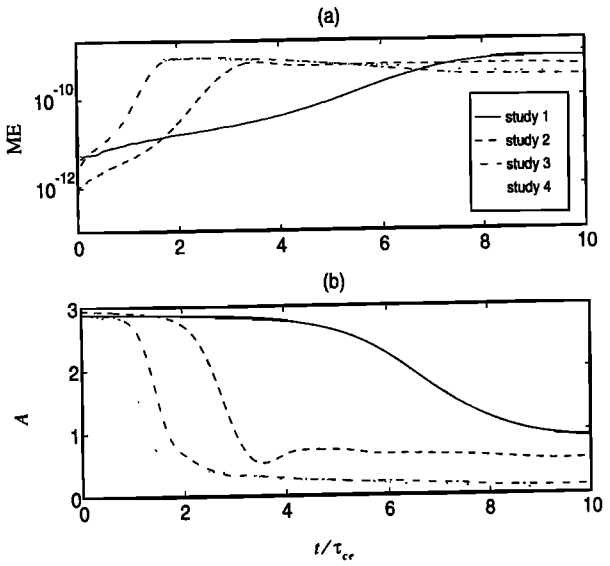

Figure 14. Variation with time of (a) magnetic wave energy density (ME) in J m^{-3} and (b) electron species anisotropy (A) in the 2-D studies.

wave amplitude in the system. As we increase $\beta_{//}$, the typical parallel electron energy required for cyclotron resonance with one of the growth wave modes in the system decreases (see the magnetic energy per particle of *Kennel and Petschek* [1966]); that is, the magnitude $|v_{//}|$ of the parallel electron velocity $v_{//}$ required for resonance decreases into a region of increasing distribution function $f(\mathbf{v})$.

As $\beta_{//}$ increases, magnetic wave energy saturates earlier (see Figures 14a and 15b), as a result of the increasing growth rates. The difference between 1-D and 2-D average growth rates, for the same $\beta_{//}$ value, becomes larger as $\beta_{//}$ increases. Again, the simulation-obtained rate of growth of magnetic wave energy density at early times are close to the mean predicted by linear theory. For example, in study 2, it is found that $\bar{\gamma}_{1D} = (0.172 \pm 0.01)\,\omega_{ce}$, $\bar{\gamma}_{2D} = (0.092 \pm 0.025)\,\omega_{ce}$, whilst the linearly-predicted mean of the growth rates of all simulation modes lying within the growth region are $0.158\,\omega_{ce}$ (1-D) and $0.123\,\omega_{ce}$ (2-D). As $\beta_{//}$ increases, more cyclotron resonances (n) become possible in 2-D (our 1-D geometry allows $n = -1$ resonance only) since the $|v_{//}|$ required for such resonances decreases (into a region of increasing $f(\mathbf{v})$), and so we might reasonably expect more differences between 1-D and 2-D results. Note that the difference between 1-D and 2-D average growth rates can be as large as by a factor ~ 2.6. Accompanying the increased wave growth rate (and hence wave amplitude as $\beta_{//}$ increases) are a more rapid decrease in the electron species anisotropy, with a lower end-of-run anisotropy level (see Figure 14b).

Along with an increasing growth rate, the normalized p.a.d. rates increase as $\beta_{//}$ increases (see Figure 16). This explains the faster rate of decrease in the electron species anisotropy as $\beta_{//}$ increases. During the growth period of wave energy, the p.a.d. rate in 1-D is larger than in 2-D for the same $\beta_{//}$ value. As $\beta_{//}$ increases, the period during which a quasi-linear approach is expected to hold shortens, since wave energy grows more rapidly (and therefore wave modes reach nonlinear amplitudes/saturation sooner). In all studies, p.a.d. rates are seen to saturate at roughly the same time as magnetic wave energy saturates, as we would expect when $\hat{D}_{\alpha k_x} \propto B_w^2$.

Strength of Pitch Angle Diffusion

To infer whether a given value of $\hat{D}_{\alpha k_x}$ implies strong or weak pitch angle diffusion is occurring, we will estimate the time taken for a magnetospheric electron to be scattered across a realistic loss cone, given that it moves in a region where the pitch angle diffusion rate is the $\hat{D}_{\alpha k_x}$ obtained from our simulations. We will then compare this time to a typical magnetospheric loss cone electron's escape time, which is the time taken for a loss cone electron to be lost to the atmosphere in the absence of scattering (typically a 1/4 bounce period). Taking a typical loss cone size at $L \sim 6$ as 3° [*Parks*, 1991], then the time taken for an initially 0° pitch angle electron to be scattered out of the loss cone is roughly $T_{LC} \sim (3)^2/D_{\alpha k_x}$, where $D_{\alpha k_x} = \hat{D}_{\alpha k} f_{ce}$ (and is then converted to units of $[\mathrm{deg}^2 \mathrm{s}^{-1}]$). A typical electron (tens of keV) on L shell ($L \sim 6$) has a bounce period T_B of a few seconds [*Parks*, 1991]. We will take a typical normalised p.a.d. rate of $\hat{D}_{\alpha k_x} = 5\times10^{-3}$ rad^2 for loss cone particles, taken from mode 5 calculations at $t \approx 2.5\tau_{ce}$ in the 2-D study 1 (since the p.a.d. rate within a mode increases with decreasing pitch angle, the p.a.d. rate for loss cone particles in a particular mode is a factor of ~3-4 times larger than that obtained by averaging over all its pitch angles, and hence this chosen value is somewhat larger than the pitch angle averaged value (Figure 10) for this time). Since the p.a.d. becomes stronger after our chosen time, a value of $\hat{D}_{\alpha k_x} = 5\times10^{-3}$ represents a lower limit to the p.a.d. occurring in these studies. A scattering time of $T_{LC} \approx 7\times10^{-5}$ s is calculated by the method described above. Assuming that a typical loss cone electron experienced this p.a.d. rate for more than about 5μsec, it would have been scattered out of the loss cone well before completing a bounce (i.e. $T_{LC} \ll T_B/4$), hence in this sense we observe strong pitch angle diffusion. Since the value of $\hat{D}_{\alpha k_x}$ on which this calculation was based represents a lower limit to the p.a.d. occurring in our simulations, it appears that, in magnet-

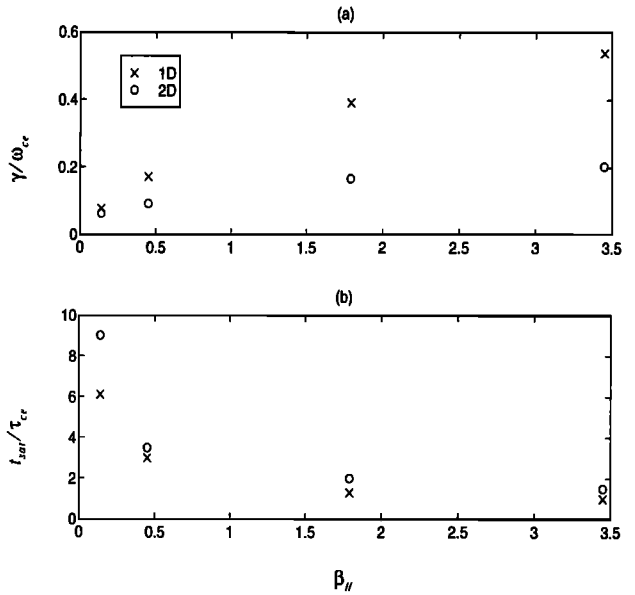

Figure 15. Variation with $\beta_{//}$ of (a) average growth rate γ and (b) saturation times t_{sat} of average magnetic wave energy in the 1-D (crosses) and 2-D (open circles) studies.

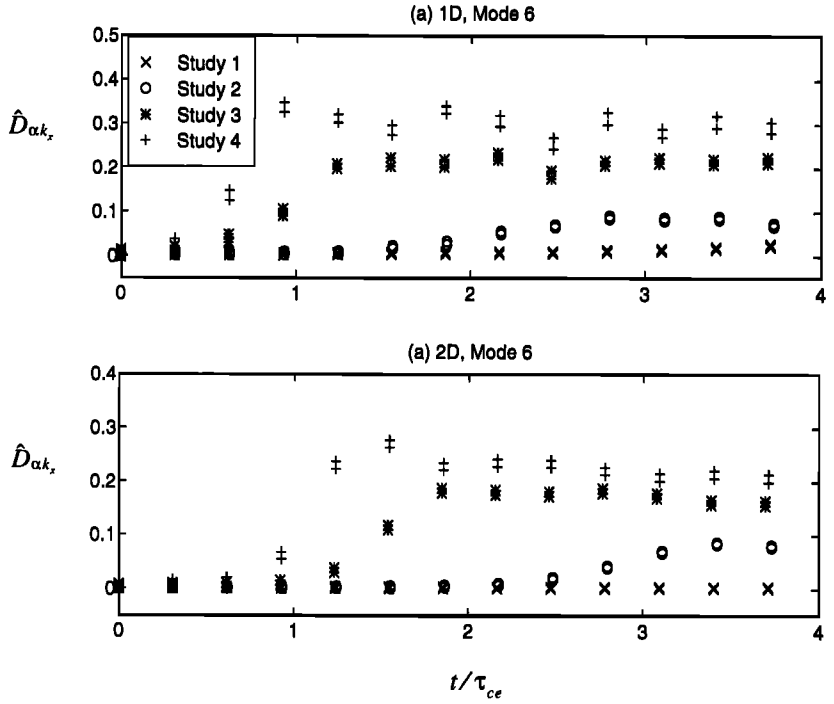

Figure 16. Normalized mode 6 pitch angle diffusion rates $\hat{D}_{\alpha k_z}$ in (a) 1-D and (b) 2-D studies.

ospheric terms, strong pitch angle diffusion occurs throughout our simulations.

Discussion

We have examined how an initially anisotropic velocity distribution ($T_\perp > T_{//}$) may lead to the growth of whistler mode waves, and the subsequent pitch angle diffusion of electrons via electron whistler mode wave-particle interactions. Our key results were: (1) As wave energy grows, the anisotropy of the resonant electron species decreases, and wave energy shifts towards lower frequency modes (generally without reaching the lowest resolved wave mode in the simulation). (2) Wave growth rates become larger as the β value of the resonant electron species increases. (3) Larger average growth rates are obtained in a 1-D geometry than in a 2-D geometry, the difference increasing as β increases, being larger by up to a factor of ~ 2.6 for the studies we performed. (4) Pitch-angle diffusion rates $\hat{D}_{\alpha k_z}$ have been found to grow as magnetic wave energy B_w^2 grows, approximately $\hat{D}_{\alpha k_z} \propto B_w^2$. (5) During the early wave growth stages of the studies, pitch angle diffusion rates are larger in a 1-D geometry, by up to a factor of ~10. (6) For the chosen parameters, strong pitch angle diffusion of electrons via WPIs occurs throughout. (7) During the early wave growth stages of the studies, resonant particles move on velocity space diffusion surfaces of constant wave frame energy, with the pitch angle diffusion for such particles being consistent with the quasi-theory of *Lyons* [1974]. (8) Pitch-angle diffusion rates increase as the β value of the resonant species increases. (9) Later in the run, particle trajectories suggest that non linear trapping of resonant particles by large amplitude electron whistler mode wave(s) may be occurring.

The effect of the shift of magnetic wave energy toward lower frequency modes is that the final wave spectrum does not exactly correspond to the linearly predicted wave spectrum. This has been previously noted in a quasi-linear theoretical treatment by *Roux and Solomon* [1971], and early one-dimensional electron whistler-instability simulations [e.g., *Ossakow et al.*, 1972]. The dependence of pitch angle diffusion rates on wave energy seems reasonable from a quasi-linear viewpoint [e.g., *Kennel and Petschek*, 1966]. The usual quasi-linear theory of resonant diffusion [*Kennel and Engelmann*, 1966] assumes negligible wave growth-rates/amplitudes ($\gamma \to 0$). Often, real wave frequencies are assumed much less than the electron cyclotron frequency ($\omega \ll \omega_{ce}$ [e.g., *Kennel and Petschek*, 1966]), which allows for an approximation of pure pitch angle diffusion. Neither of these conditions are characteristic of the simulations presented here (growth rates and real wave frequencies are both a significant fraction of ω_{ce}, see Figures 2 and 3). Nevertheless, at early stages in the simulations, resonant particle wave frame energies and the variation of the p.a.d. rate as a function of pitch angle within a resonant region of v space suggests that resonant particles diffuse along surfaces of constant energy measured in the wave frame, with a pure pitch angle diffusion description sufficing below pitch angles about $\alpha < 50°$. It thus appears that a quasi-linear description of the p.a.d. process seems reasonable during the early stages of the simulations, during which wave energies have not grown to large nonlinear amplitudes. Later in the simulations, when the wave spectrum has become dominated by a single large-amplitude wave mode, particle trajectories indicate that nonlinear trapping of particles may be occurring. Analysis of particle trajectories and a study of trapping in the nonlinear regime of the simulations have been performed and will be reported in a separate paper. Such effects may play an important role in the overall saturation of wave energy seen in the simulation studies. We do not expect such a saturation mechanism to be too important in the magnetospheric problem of

pitch angle diffusion due to whistler mode turbulence, since wave loss from the wave-growth region becomes an important factor in determining saturation, and our simulations have not modeled such a loss. However, a simulation study of trapping effects may prove to be of some use in situations where the wave-particle interactions are coherent and nonlinear (as opposed to the quasi-linear turbulent case more usually treated), which may play some role in the generation of magnetospheric VLF triggered emissions, as reviewed by *Matsumoto* [1979].

Our simulation parameters were chosen to be of interest to the problem of whistler mode wave growth from and pitch angle diffusion of anisotropic energetic electron distributions that are injected into the nightside ring current region under an enhanced cross-tail electric field during magnetically disturbed times [e.g., *Ashour-Abdalla & Cowley*, 1974; *Kremser et al.*, 1986]. Our study 1 parameters are representative of the plasmapause region on the nightside during geomagnetically disturbed times. Note a rather large anisotropy (temperature ratio $T_\perp/T_{//} \approx 4$) was used to overcome non-whistler noise levels inherent in 2-D electromagnetic particle-in-cell simulations ($T_\perp/T_{//} \approx 1.5-2$ appearing to be more magnetospherically reasonable [e.g., *Kremser et al.*, 1986]). Higher β value studies (β from approximately 4 to 30) contain an electron species of unrealistically large β value in magnetospheric terms and were made to investigate the effects of increasing β on the physics of the instability. Since the 1-D/2-D simulations presented here cover a wide range of parameters (electron temperature, background magnetic field strength), they are also of general interest to a linear and nonlinear understanding of the whistler mode instability and electron whistler wave-particle interactions. In all simulations we found, for a given initial electron distribution and background magnetic field (given β value), the timescale for pitch angle diffusion in a 2-D geometry to be greater than that in a 1-D geometry (lower p.a.d. rates in 2-D), thereby indicating the need for inclusion of both parallel and oblique propagating whistler waves in a 2-D geometry for a proper treatment of the wave growth and electron pitch angle diffusion associated with the electron whistler mode instability. Our results also show that, during the wave growth period of the instability, the quasi-linear picture of velocity space diffusion along surfaces of constant wave frame energy [e.g., *Lyons*, 1974] to be valid, even when growth-rates are not negligible, several wave modes (both parallel and oblique) are growing simultaneously (2-D wave propagation) and relatively large real wave-frequencies exist. In addition, even when the ratio of wave-phase velocity (v_ϕ) to resonant electron parallel-velocity ($v_{//res}$) is not negligible ($|v_\phi/v_{//res}| \sim 1$ typical here), a pure pitch angle diffusion description of velocity space diffusion appears to be appropriate for pitch angles below about $\alpha < 50°$. The simplifications present in our simulations, relative to the magnetospheric problem, need to be borne in mind. Our simulations were essentially performed in a closed box (periodic boundary conditions) from which no particle or wave energy loss occurs, and in which a discrete set of simulation wave modes are allowed. As outlined at the beginning of the paper, our results are not found to be affected by including a realistic loss cone sink for particles at the boundaries of the simulation box, since so few simulation particles fall within a realistic loss cone (typically ~5° for the plasma sheet; note our simulations are not loss cone driven, the loss cone sink consideration is purely to allow the robustness of our results with respect to particle loss to be evaluated). Effects of wave energy loss at the simulation boundaries on the evolution of the instability are less clear and are suggested as future work at the end of the discussion. Nevertheless, since the quasi-linear aspects of our simulation results are taken from the early part of the simulation (first 4-5τ_{ce} electron gyroperiods), during which time we do not believe a great deal of wave loss from the simulation region would occur (based on the linearly predicted wave phase-velocities, the transit time of a whistler wave across our simulation box being ~8-9 τ_{ce}), we do not feel the quasi-linear aspects of our results would be significantly affected by a boundary wave loss (for the parameters used in these studies).

An understanding of the magnetospheric problem outlined above has relevance to an understanding of the disturbed time aurora. Recent interest in the pitch angle diffusion due to electron whistler WPIs has also been in the question of which wave modes are responsible for the electron precipitation forming the diffuse aurora. It is now generally acknowledged that the precipitation of electrons forming the diffuse aurora is unlikely to be a result of pitch angle diffusion due to electron-cyclotron harmonic wave-particle interactions, since observed electric field strengths are too low to account for the observed intensities of low energy (less than 10 keV energies) diffuse auroral electrons [e.g., *Belmont et al.*, 1983; *Roeder and Koons*, 1989]. *Johnstone et al.* [1993] (hereinafter referred to as JWLH) have recently proposed electron whistler wave pitch angle diffusion as a candidate for the precipitation mechanism of low energy electrons (<10 keV) into the auroral loss cone. In JWLH, a "diffusive equilibrium" model was employed to represent the continuous precipitation of electrons, in which wave growth from an unstable loss cone distribution of electrons balances wave losses, and electron injection at large pitch angles balances electron precipitation through the loss cone. This model requires both a loss of wave energy and particles from the interaction region. Our simulations were designed to investigate nonequilibrium substorm-injected electron distributions, rather than a loss cone distribution, have no absorption of waves at the boundaries, and are therefore not directly applicable to JWLH's paper. However, we believe there to be two results from our simulations of interest to JWLH's proposal. First, our simulations show that strong pitch angle diffusion (in magnetospheric terms) of resonant electrons having energies below 10 keV can occur via electron whistler wave-particle interactions. The electrons resonant with mode 7 in our study 1 (see Figures 10 and 13 for the pitch angle diffusion rates of mode 7 resonant electrons) have minimum resonant energies $1/2 m_e v^2_{//res} \approx 3.9$ keV, being resonant with a whistler wave mode at a frequency $\omega \approx 0.67\omega_{ce}$. Wave mode 7 is a linearly predicted growth mode in our study 1, and although it is not the dominant mode in the wave spectrum, it contains significant magnetic energy over the chosen quasi-linear time period (see Figures 5 and 8). Significant wave energy at such relatively high wave-frequencies (say $\omega > 0.5\omega_{ce}$) allows the pitch angle diffusion of electrons having energies much lower than considered in the past (where $\omega \ll \omega_{ce}$ was the usual assumption [e.g., *Kennel and Petschek*, 1966]. This is heavily stressed in JWLH, in fact, it is vital for the pitch angle diffusion of low energy electrons to occur. Our simulations show that it is possible to cause strong

pitch angle diffusion of low-energy (<10 keV) electrons via such WPIs, provided there is significant wave-energy present over the resonant frequency range, and hence a consideration of the wave data is necessary in proposing electron whistler WPIs as a low-energy electron precipitation mechanism. Since the wave data were not presented in JWLH, the interesting question of which wave mode is responsible for continuous auroral precipitation remains open. Second, JWLH relied on electron velocity space diffusion along diffusion curves of constant wave frame energy, assuming a wave spectrum containing parallel propagating whistler-waves only, and (JWLH, p. 5963) questioned "whether the electrons interact with whistler noise and diffuse along these curves or not" when a full wave spectrum including obliquely propagating waves is actually present (usually such curves are derived only for a single wave mode at a single frequency [e.g., *Kennel & Engelmann*, 1966]. Both our 1-D and 2-D results were consistent with electron diffusion along the surfaces of constant wave frame energy and may therefore provide an answer to such a question.

Future simulation work regarding the electron whistler-instability may therefore involve: (1) opening the boundaries of the simulation region to allow both wave and particle loss, (2) reduction of noise levels to allow simulations with more realistic anisotropies, (3) use of typically observed magnetospheric energetic electron distributions, such as contained in the CRRES low energy plasma analyzer (LEPA) satellite data set [*Hardy et al.*, 1993], and (4) inclusion of a varying amount of cold plasma and its effects on the electron whistler instability, all of which are expected to make a simulation-based investigation of the magnetospheric electron pitch angle diffusion problem more realistic.

Acknowledgments. P. Devine was supported by a PPARC research studentship. The European Simulation Network funded in part the development of the simulation code. We would like to acknowledge I. Roth of Berkeley for providing the XWHAMP code, developed at Dartmouth College, New Hampshire, under the Northstar project. XWHAMP is based on K. Ronnmark's original WHAMP code.

The Editor thanks Hiroshi Matsumoto and David Schriver for their assistance in evaluating this paper.

References

Ashour-Abdalla, M., and S.W.H. Cowley, Wave-particle interactions near the geostationary orbit, in *Magnetospheric Physics*, edited by B.M. McCormac, pp. 241-270, D. Reidel, Norwell, Mass., Dordrecht-Holland, 1974.

Belmont, G., D. Fontaine, and P. Canu, Are equatorial electron cyclotron waves responsible for diffuse auroral electron precipitation?, *J. Geophys. Res., 88*, 9163-9170, 1983.

Birdsall, C.K., and A.B. Langdon, *Plasma Physics via Computer Simulation*, McGraw-Hill, New York, 1985.

Cuperman, S., and Y. Salu, Magnetospheric implications of the nonlinear whistler instability obtained in a computer experiment, *J. Geophys. Res., 78*, 4792-4796, 1973.

Cuperman, S., and A. Sternlieb, Obliquely propagating unstable whistler waves: a computer simulation, *J. Plasma Phys., 11*, 175-188, 1974.

Dungey, J., The loss of Van Allen electrons due to whistlers, *Planet. Space Sci., 11*, 591-595, 1963.

Eastwood, J.W., The virtual particle electromagnetic particle-mesh method, *Comput. Phys. Commun., 64*, 252-266, 1991.

Hardy, D.A., D.M. Walton, A.D. Johnstone, M.F. Smith, M.P. Gough, A. Huber, J.Pantazis, and R. Burkhardt, Low-energy plasma analyzer, *IEEE Trans. Nucl. Sci., 40*(2), 246-251, 1993.

Johnstone, A.D., D.M. Walton, R. Liu, and D.A. Hardy, Pitch angle diffusion of low energy electrons by whistler mod waves, *J. Geophys. Res., 98*, 5959-5967, 1993.

Kennel, C.F., and F. Engelmann, Velocity space diffusion from weak plasma turbulence in a magnetic field, *Phys. Fluids 9*(12), 2377-2388, 1966.

Kennel, C.F., and H.E. Petschek, Limit on stably trapped particle fluxes, *J. Geophys. Res., 71*, 1-28, 1966.

Kremser, G., et al., Energetic electron precipitation during a magnetospheric substorm and its relationship to wave particle interaction, *J. Geophys. Res., 91*, 5711-5718, 1986.

Lyons, L.R., General relations for resonant particle diffusion in pitch angle and energy, *J. Plasma Phys., 12*, 1, 45-49, 1974.

Lyons, L.R., R.M. Thorne, and C.F. Kennel, Pitch angle diffusion of radiation belt electrons within the plasmasphere, *J. Geophys. Res. 77*, 3455-3474, 1972.

Matsumoto, H., Nonlinear whistler-mode interaction and triggered emissions in the magnetosphere: a review, in *Wave Instabilities in Space Plasmas*, edited by P.J. Palmadesso and K. Papadopoulos, p.p. 163-190, D. Reidel, Norwell, Mass., 1979.

Matsumoto, H., M. Ohashi, and Y. Omura, A computer simulation study of hook-induced electrostatic bursts observed in the magnetosphere by the ISEE satellite, *J. Geophys. Res., 89*, 3873-3881, 1984.

Ossakow, S.L., E. Ott, and I. Haber, Nonlinear evolution of whistler instabilities, *Phys. Fluids, 15*, 2314-2326, 1972.

Parks, G.K., *Physics of Space Plasmas: An Introduction*, Addison-Wesley, Reading, Mass., 1991.

Pritchett, P.L., D. Schriver, and M. Ashour-Abdalla, Simulation of whistler waves excited in the presence of a cold plasma cloud: Implications for the CRRES mission, *J. Geophys. Res., 96*, 19,507-19,512, 1991.

Roeder, J.L., and H.C. Koons, A survey of electron cyclotron waves in the magnetosphere and the diffuse auroral electron precipitation, *J. Geophys. Res., 94*, 2529-2541, 1989.

Ronnmark, K., WHAMP- Waves in homogeneous, anisotropic, multi-component plasmas, *KGI Rep. 179*, Kiruna Geophysical Institute, Kiruna, Sweden, June 1982.

Roux, A., and J. Solomon, Self-consistent solution of the quasi-linear theory: Application to the spectral shape and intensity of VLF waves in the magnetosphere, *J. Atmos. Terr. Phys., 33*, 1457-1471, 1971.

Stix, T., *The Theory of Waves in Plasma*, McGraw-Hill, New York, 1962.

Sudan, R.N., and E. Ott, Theory of triggered VLF emissions, *J. Geophys. Res., 76*, 4463-4476, 1971.

Zhang, Y.L., H. Matsumoto, and Y. Omura, Linear and nonlinear interactions of an electron beam with oblique whistler and electrostatic waves in the magnetosphere, *J. Geophys. Res., 98*, 21,353-21,363, 1993.

P. E. Devine and S. C. Chapman, Physics and Astronomy Subject Group, Space Science Centre, School of Mathematical and Physical Sciences, University of Sussex, Falmer, Brighton BN1 9QH, England. (e-mail: pauldv@sussex.ac.uk; S.C.Chapman@sussex.ac.uk)

J. W. Eastwood, AEA Technology, Culham Laboratory, Abingdon, Oxfordshire OX14 3DB, England. (e-mail: jim.eastwood@aea.orgn.uk)

(Received August 30, 1994; revised March 8, 1995; accepted March 8, 1995.)